Materials & Design 214 (2022) 110382

Contents lists available at ScienceDirect

Materials & Design

journal homepage: www.elsevier.com/locate/matdes

Mechanically robust $Ti_3C_2T_x$ MXene/Carbon fiber fabric/Thermoplastic polyurethane composite for efficient electromagnetic interference shielding applications

Ningmin Duan [a,b], Zhenyu Shi [a,b,*], Zhaohui Wang [a,b], Bin Zou [a,b], Chengpeng Zhang [a,b], Jilai Wang [a,b], Jianren Xi [c], Xiaoshuai Zhang [d], Xianzhi Zhang [e], Guilong Wang [c,f,*]

[a] Key Laboratory of High Efficiency and Clean Mechanical Manufacture (Ministry of Education), Shandong University, Jinan, Shandong 250061, China
[b] School of Mechanical Engineering, Shandong University, Jinan, China
[c] School of Materials Science and Engineering, Shandong University, Jinan, China
[d] Department of Science and Technology Management, Shandong University, Jinan, China
[e] School of Engineering and Environment, Kingston University, London, UK
[f] Key Laboratory for Liquid-Solid Structural Evolution and Processing of Materials (Ministry of Education), Shandong University, Jinan, Shandong 250061, China

HIGHLIGHTS

- The composite was prepared by electrohydrodynamic atomization deposition, layer-by-layer stacking and hot pressing technology.
- The synergistic strengthening effect of van der Waals forces and covalent bonds improved the tensile strength of the composite.
- The composite showed outstanding resistance stability, flexibility and electromagnetic interference shielding stability.

GRAPHICAL ABSTRACT

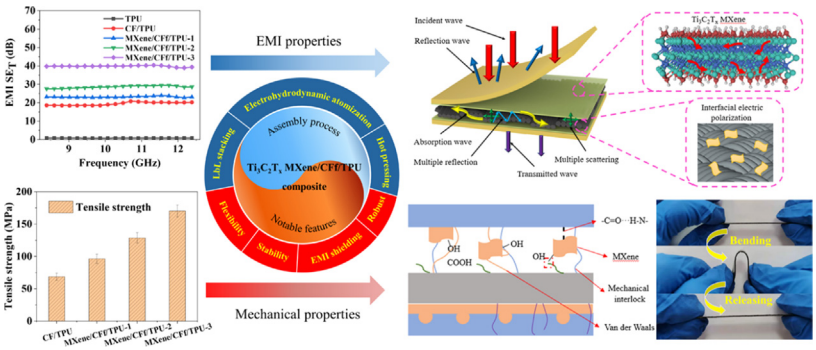

ARTICLE INFO

Article history:
Received 29 September 2021
Revised 21 December 2021
Accepted 3 January 2022
Available online 05 January 2022

Keywords:
$Ti_3C_2T_x$ MXene
Flexibility
Stability
Electrohydrodynamic atomization deposition
Electromagnetic interference shielding
Mechanical property

ABSTRACT

It is a challenge to design $Ti_3C_2T_x$ MXene-based electromagnetic interference (EMI) shielding composites with excellent mechanical properties. Herein, a highly robust, flexible and durable $Ti_3C_2T_x$ MXene/carbon fiber fabric/thermoplastic polyurethanes ($Ti_3C_2T_x$ MXene/CFf/TPU) composite was fabricated through simple electrohydrodynamic atomization deposition, layer-by-layer stacking and hot pressing technology. The synergistic strengthening effect of van der Waals forces and covalent bonds can improve the tensile strength of the composite up to170.2 MPa, which is far greater than that of other MXene-based composites previously reported. In addition, the EMI shielding performance of the $Ti_3C_2T_x$ MXene/CFf/TPU composite also improved with increasing MXene mass fraction, reaching 40.4 dB, which can be attributed to the dielectric loss provided by conductive fillers and the enhanced absorption within the sandwich structure. More interestingly, the composite retained excellent resistance stability, EMI-SE stability and flexibility, even after multiple bending and releasing cycles. This work provides a facile and environmentally-friendly method for preparing composites with excellent EMI shielding properties and mechanical properties, which may provide more possibilities for applications in intelligent wear and electronic wireless communication equipment.

* Corresponding authors at: Key Laboratory of High Efficiency and Clean Mechanical Manufacture (Ministry of Education), Shandong University, Jinan, Shandong 250061, China (Z. Shi) School of Materials Science and Engineering, Shandong University, Jinan, China (G. Wang).
E-mail addresses: shizhenyu@sdu.edu.cn (Z. Shi), guilong@sdu.edu.cn (G. Wang).

https://doi.org/10.1016/j.matdes.2022.110382

1. Introduction

In recent years, the development of flexible wearable products and wireless communication technology has made electromagnetic interference become an inevitable problem [1–4]. Currently, commonly used metal materials have the characteristics of low flexibility, high density and susceptibility to corrosion, which make it difficult to meet the increasing EMI demand. Polymer composites possess the advantages of good flexibility, light weight, low cost and chemical stability, which are considered to be suitable for application in flexible electronic products [5–8]. To date, researchers have done outstanding work in the development of lightweight EMI shielding materials [9–11]. For example, Zhang et al. fabricated a polydimethylsilane/reduced graphene oxide/single-wall carbon nanotube nanocomposite, and found that the electromagnetic interference shielding effectiveness (EMI-SE) of the nanocomposite could reach 31 dB [9]. Chen et al. manufactured a lightweight and flexible graphene foam composite. The EMI-SE of the composite remained stable even after multiple bending cycles [10]. Although many polymer materials have satisfactory electromagnetic shielding properties, poor ductility and complex preparation process limit their application in electronic products, and their mechanical properties and EMI shielding properties need to be further improved [12,13].

Recently, two-dimensional transition metal carbides and nitrides (MXenes) have received considerable attention, due to their unique layered structure, metal-like conductivity and hydrophilic surface characteristics [14]. MXene materials have many surface groups, such as OH, O and F, and it is the presence of abundant surface ends on MXene materials that enable them to be dispersed over many substrates [15]. Therefore, MXene materials will be a strong competitor in the next generation of EMI shielding materials [13,16]. Wang et al. used multilayered casting to fabricate the poly (vinyl alcohol)/MXene composites, with the EMI-SE reaching 44.8 dB for a composite thickness of 27 μm. Furthermore, a multilayered structure is conducive to absorption and reflection of electromagnetic microwaves [17]. Various MXene/natural rubber nanocomposite films with excellent flexibility and electrical conduction properties have also been reported [18], the film with a 6.71 vol% MXene loading exhibited an EMI-SE of 53.6 dB, and a tensile strength of approximately 19 MPa owing to the enhanced interface interaction. Wei et al. prepared a $Ti_3C_2T_x$ MXene/aramid nanofiber (ANF) composite, with a $Ti_3C_2T_x$ MXene to ANFs mass ratio of 1:1, which exhibited a tensile strength of 116.71 MPa [19]. Although these outstanding achievements undoubtedly provide more possibilities for building lighter EMI materials, there remains considerable scope for improving the mechanical properties of EMI shielding materials, which is one of the problems with MXene-based composites that may limit their application to wearable and flexible electronic products [20,21]. To meet the mechanical property requirements of EMI shielding materials in electronic products, the design of new EMI shielding materials with excellent mechanical properties is urgently required.

Herein, to solve the problem of insufficient strength of the MXene-based composites, highly robust, flexible and durable $Ti_3C_2T_x$ MXene/carbon fiber fabric/thermoplastic polyurethanes ($Ti_3C_2T_x$ MXene/CFf/TPU) composites were prepared through electrohydrodynamic atomization (EHDA) deposition, hot pressing and layer-by-layer stacking technology. Through ordinary atomization deposition, two-dimensional $Ti_3C_2T_x$ nanosheets were well-distributed on the surface of the CF fabric. The MXene content can be controlled by changing the number of atomization deposition cycles. The tensile strength of the $Ti_3C_2T_x$ MXene/CFf/TPU composite reached a maximum of 170.2 MPa, which is far better than that of many other competitive MXene-based materials. The main damage modes of the $Ti_3C_2T_x$ MXene/CFf/TPU composite were interfacial debonding and fiber breakage. The EMI shielding performance and shielding mechanism of the $Ti_3C_2T_x$ MXene/CFf/TPU composite were also analyzed. The EMI-SE of the $Ti_3C_2T_x$ MXene/CFf/TPU composite can reach 40.4 dB, which can perfectly meet the commercial standard for shielding effectiveness of EMI materials. More interestingly, the composite prepared in our work also shows excellent resistance stability, EMI-SE stability and flexibility even after multiple bending and releasing cycles.

2. Experimental

2.1. Materials

Ti_3AlC_2 powder (38 μm, 98% purity) was obtained from Jilin 11 Technology Co., Ltd. Concentrated hydrochloric acid (HCl), concentrated nitric acid (HNO_3), acetone and lithium fluoride (LiF) were purchased from Shanghai Aladdin Biochemical Technology Co., Ltd. Carbon fiber fabric (CFf) was supplied by Yixing Luote Carbon Fiber Weaving Co., Ltd. Thermoplastic polyurethane elastomer (BTE-75A) was provided by Shandong Yousuo Chemical Technology Co., Ltd.

2.2. Preparation of the $Ti_3C_2T_x$ MXene colloidal solution

Ti_3C_2Tx MXene was prepared by a modified etching method [22,23]. First, LiF (2 g) was dissolved in HCl (25 mL) in a beaker. Ti_3AlC_2 (1.3 g) was then added to the mixed solution, and the beaker was heated to 40 °C for 24 h. After that, the products were washed with deionized water and centrifuged at 3500 rpm for 5 min. The centrifugation was performed eight times. Deionized water was then mixed with the precipitate to prepare a 150 mL dispersion by manual shaking. The dispersion was then centrifuged at 3500 rpm for more than 1 h, and the supernatant, corresponding to a dispersion of few-layer or single layer Ti3C2Tx MXene, was collected for further use.

2.3. Fabrication of lightweight $Ti_3C_2T_x$ MXene/CFf/TPU composites

A schematic of the $Ti_3C_2T_x$ MXene/CFf/TPU composite preparation process is shown in Fig. 1a. The CF fabric was first placed in acetone reflux for 24 h, and then repeatedly washed in deionized water and dried to obtain the desizing CF fabric. To introduce more oxygen-containing functional groups on the surface of the CF fabric, the desizing CF fabric was treated in a concentrated nitric acid solution at 70 °C for 1 h. The treated CF fabric was washed five times with deionized water and then dried in a vacuum oven at 100 °C for 24 h. The electrohydrodynamic atomization is a simple and effective deposition method [24,25]. The device mainly consisted of a stainless steel needle, a syringe pump, a power supply and a motion platform. The outlet of the atomizing needle was connected to the power supply through a metal wire, and the MXene dispersion was sprayed out. The distance between the nozzle and CF fabric was 20 cm. During the atomization deposition process, the nozzle moved back and forth at a speed of approximately 5 cm/s to ensure complete and uniform coverage. As shown in

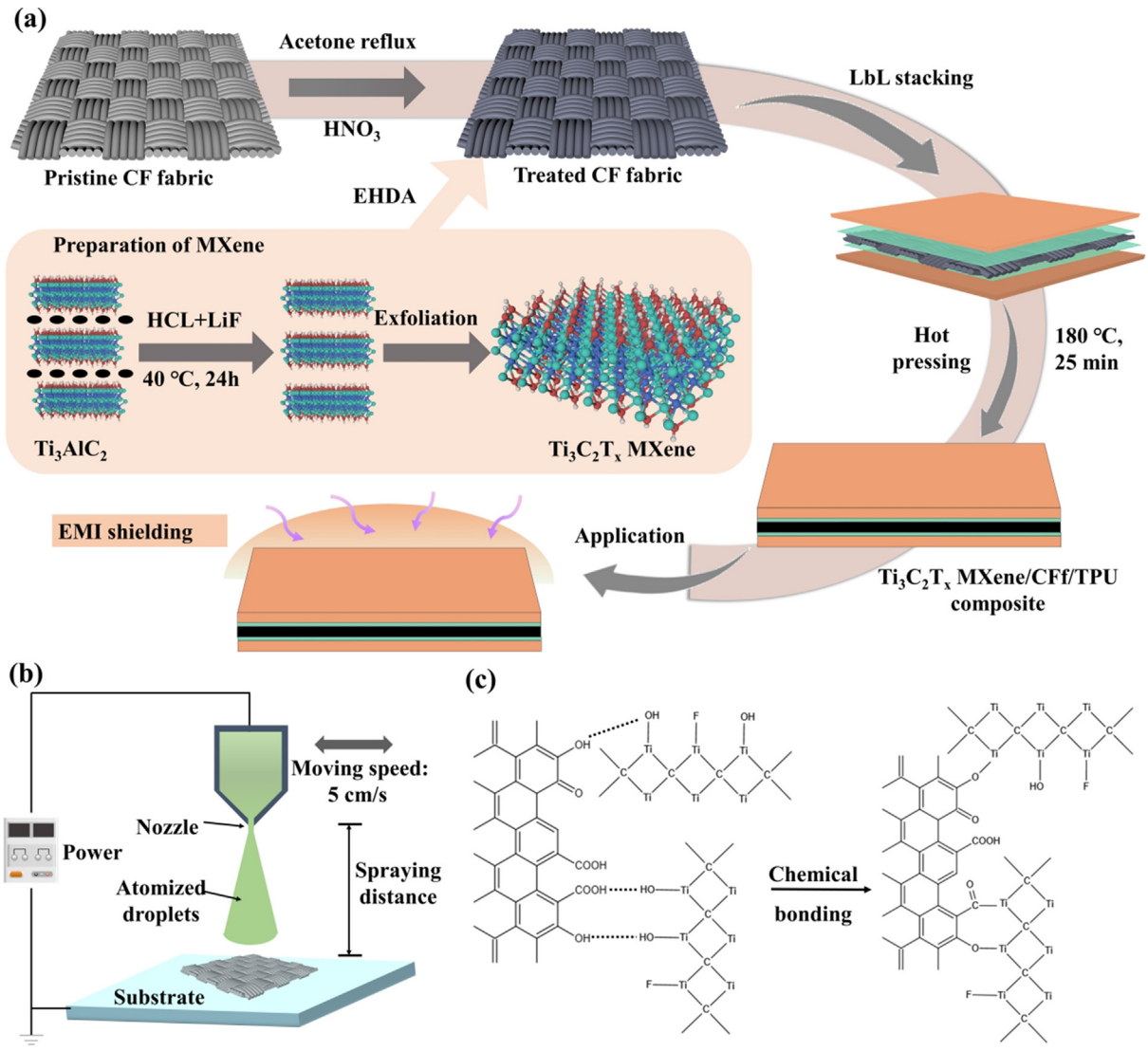

Fig. 1. (a) A schematic of the $Ti_3C_2T_x$ MXene/CFf/TPU composite preparation process; (b) Schematic diagram of the EHDA deposition; (c) Chemical reaction on the surface of CF fabric.

Fig. 1b, the $Ti_3C_2T_x$ MXene solution was uniformly atomized on one side of the CF fabric, and then dried at 50 °C for 1 h. Subsequently, the other side of the CF fabric was treated in the same way. The weight ratios of MXene in the MXene/CF fabric were calculated to be approximately 0.32%, 0.57% and 1.06%, which can be denoted as MXene/CFf-1, MXene/CFf-2 and MXene/CFf-3, respectively. The chemical reactions on the surface of the CF fabric are shown in Fig. 1c. New bonding interactions facilitate the combination of MXene and TPU.

The $Ti_3C_2T_x$ MXene/CFf/TPU composites were subsequently fabricated by hot pressing and layer-by-layer stacking. MXene/CFf-1 was placed between two TPU plates, forming a sandwich structure. They were covered tightly with greaseproof paper, and then placed on a hot-press device for high-temperature and high-pressure treatment comprising hot-pressing at 180 °C and 8 MPa for 25 min. Hot pressing is a very good method to prevent oxidation. Under a pressure of 8 MPa, the CF fabric coated with MXene was tightly clamped by TPU, and MXene molecules were not in direct contact with air, similar to a vacuum environment. Thus, the oxidation of MXene under high temperatures can be effectively avoided. After treatment, the samples were cooled at room temperature, completing the fabrication of the $Ti_3C_2T_x$ MXene/CFf-1/TPU composite, which can be denoted as $Ti_3C_2T_x$ MXene/CFf/TPU-1. The $Ti_3C_2T_x$ MXene/CFf-2 and $Ti_3C_2T_x$ MXene/CFf-3 composites were obtained similarly.

2.4. Characterization

2.4.1. Scanning electron microscopy

The morphologies of $Ti_3C_2T_x$ MXene, CF and the $Ti_3C_2T_x$ MXene/CFf/TPU composites were studied using scanning electron microscopy (SEM, JSM-6610LV) with an acceleration voltage of 10 kV.

2.4.2. Fourier transform infrared spectroscopy

The surface groups of $Ti_3C_2T_x$ MXene/CFf were examined using Fourier transform infrared spectroscopy (FTIR, Nicolet iS50). The FTIR spectrum of the sample was collected in the range of 400–4000 cm^{-1}, with a resolution of 4 cm^{-1}.

2.4.3. X-ray photoelectron spectroscopy

X-ray photoelectron spectroscopy (XPS) was performed using an X-ray photoelectron spectrometer (Thermo ESCALAB 250XI) with an Al Kα X-ray source. The voltage was 15 kV and the power

was 600 W. The samples were vacuum-dried for 24 h before testing.

2.4.4. Transmission electron microscopy

Transmission electron microscopy (TEM, JEM-2100) was used to investigate the morphologies of the $Ti_3C_2T_x$ MXene using an acceleration voltage of 200 kV.

2.4.5. Electrical conductivity measurement

The RTS-8 four-probe resistivity meter (Guangzhou Four Probe Technology Co., Ltd.) was used to test the sheet resistance and conductivity of the composites. Each sample was tested ten times to reduce the error and the average value was taken.

2.4.6. Mechanical property measurement

The tensile strength and interlaminar shear strength were measured using an electronic universal tensile testing machine (ME0030, Shenzhen Senke Xinchuang Technology Co., Ltd.). All the tests were conducted at a speed of 5 mm/min. The tensile tests were conducted according to the ASTM D 3039 standard. The interlaminar shear tests were conducted according to the GB-T 15598–1995 standard. Each sample was tested at least five times.

2.4.7. EMI shielding measurement

The S parameters were measured using a vector network analyzer (N5234A, Agilent, USA). The size of the specimen was 22.86 mm × 10.16 mm × 0.5 mm. The waveguide method was adopted to test over a frequency range of 8.2–12.4 GHz. The calculation formula is as follows [11]:

$$SE = SE_A + SE_R + SE_M$$

$$R = |S_{11}|^2 = |S_{22}|^2 \quad (2)$$

$$T = |S_{21}|^2 = |S_{12}|^2 \quad (3)$$

$$A = (1 - R - T) \quad (4)$$

$$SE_R = -10\log(1 - R) \quad (5)$$

$$SE_A = -10\log(1 - A) = -10\log[T/(1 - R)] \quad (6)$$

T, R, and A are the transmission coefficient, reflection coefficient and absorption coefficient, respectively. When SE_T is greater than 15 dB, SE_M is usually neglected [26].

3. Results and discussion

3.1. Morphology and structure characterization

Fig. 2a presents the SEM image of $Ti_3C_2T_x$ MXene. Uniformly exfoliated MXene layers were obtained from a diluted $Ti_3C_2T_x$ colloidal solution on a silicon wafer. The TEM images of $Ti_3C_2T_x$ MXene are shown in Fig. 2b–c. Interestingly, the prepared $Ti_3C_2T_x$ MXene suspensions displayed an obvious Tyndall effect, which indicates that $Ti_3C_2T_x$ exhibits stable and excellent dispersibility in aqueous solution (Fig. 2b). As shown in Fig. 2c, the thickness of the exfoliated $Ti_3C_2T_x$ flakes was approximately 1.03 nm. The SEM images of CF with different mass fractions of $Ti_3C_2T_x$ are shown in Fig. 2d–g. The surface of untreated CF was relatively smooth, and there were no gullies and other defects (Fig. 2d). When $Ti_3C_2T_x$ flakes were deposited on the surface of the CF, the surface became rougher, and as the mass fraction increased from 0.32 wt% to 1.06 wt%, this phenomenon becomes progressively more obvious. As shown in Fig. 2g, $Ti_3C_2T_x$ MXene was uniformly deposited on the CF surface for a mass fraction of 1.06 wt%. Furthermore, the chemical composition of the CF surface coated with MXene was analyzed by elemental mapping, as shown in Fig. S1. The distribution and content of C, O and Ti elements can be seen in the EDS hierarchical diagram. Fig. 2h-i shows the cross-sectional views of the $Ti_3C_2T_x$ MXene/CFf/TPU composite. The composite had an obvious layered structure, similar to a sandwich structure. Because the single layer CF fabric is woven orthogonally, there will be horizontal and vertical tows. In some areas, the TPU melt completely covered the CF. The resin infiltration into the fiber interior enhanced bonding, which directly affects the performance of the composite. To roughly study the infiltration effect of TPU melt, a simple penetration infiltration model was used for the analysis. Darcy's law is usually used for its penetration mode infiltration model [27] as follows:

$$\frac{dz}{dt} = \frac{Kp}{\eta}\frac{dP}{dz} \quad (7)$$

$$z = \sqrt{\frac{2PK_pt}{\eta}} \quad (8)$$

Where z is the infiltration distance, t is the infiltration time, K_p is the transverse permeability of the CF bundle, η is the viscosity of the TPU melt, and P is the pressure.

The Gebart formula is commonly used to calculate the K_p of fiber-reinforced composites [28].

$$K_P = C_1\left(\sqrt{\frac{V_{f,max}}{V_f}} - 1\right)^{2.5} R_f^2 \quad (9)$$

V_f is the fiber volume content in the fiber bundle, and R_f is the radius of the fiber monofilament. There are two main types of fiber arrangements, a quadrilateral arrangement and a hexagonal arrangement. These values are listed in Table 1.

According to the calculation, K_p is 3.414 × 10^{-14} m^2 and z is 54 μm. From Fig. 2h, the average thickness of the CF layer is 196 μm, and the thickness of the CF fabric used in this study is 0.29 mm, it can be concluded that the actual infiltration thickness was 47 μm, which is slightly less than the theoretically simulated infiltration thickness. This may be due to the existence of MXene, which affected the infiltration of the TPU melt, as the MXene layer was completely infiltrated by the melt TPU. Overall, the molten TPU was well infiltrated inside the CF bundles under high temperature and pressure conditions. This provides a basis for improving the performance of the composites.

3.2. FTIR and XPS analysis

The FTIR spectra of $Ti_3C_2T_x$ MXene and $Ti_3C_2T_x$ MXene/CF nanocomposites are shown in Fig. 3a. In the FTIR spectrum of $Ti_3C_2T_x$, the characteristic peaks at 3437 cm^{-1} and 551 cm^{-1} correspond to the stretching vibration of O—H. The peaks at 1614 cm^{-1} and 1388 cm^{-1} can be assigned to the stretching vibrations of C═O and C—F, respectively. After $Ti_3C_2T_x$ MXene was evenly distributed on the CF fabric, the typical peaks of the $Ti_3C_2T_x$ MXene/CFf nanocomposite include the stretching vibration of O-H (3413 cm^{-1} and 555 cm^{-1}), C═O (1625 cm^{-1}) and C—F (1380 cm^{-1}). The strong absorption peak at 756 cm^{-1} is ascribed to the C-H bending vibration in double bonds [29]. Fig. 3b shows the XPS spectra of $Ti_3C_2T_x$ MXene and the $Ti_3C_2T_x$ MXene/CFf nanocomposites. The elements of C, O, Ti, and F can be clearly seen. In the spectra of Ti 2p (Fig. 3c), the peaks at ~ 455.5 eV, 456.1 eV, 457.3 eV, 459.8 eV, 461.9 eV and 463.1 eV can be attributed to the Ti—C—T_x ($2p_{3/2}$), Ti (II) ($2p_{3/2}$), Ti-O ($2p_{3/2}$), Ti-C-T_x ($2p_{1/2}$), Ti (II) ($2p_{1/2}$) and Ti—O ($2p_{1/2}$) bonds, respectively. In the spectra of O 1s spectra (Fig. 3d), the peaks at ~ 529.4 eV, 530.3 eV, 532.3 eV

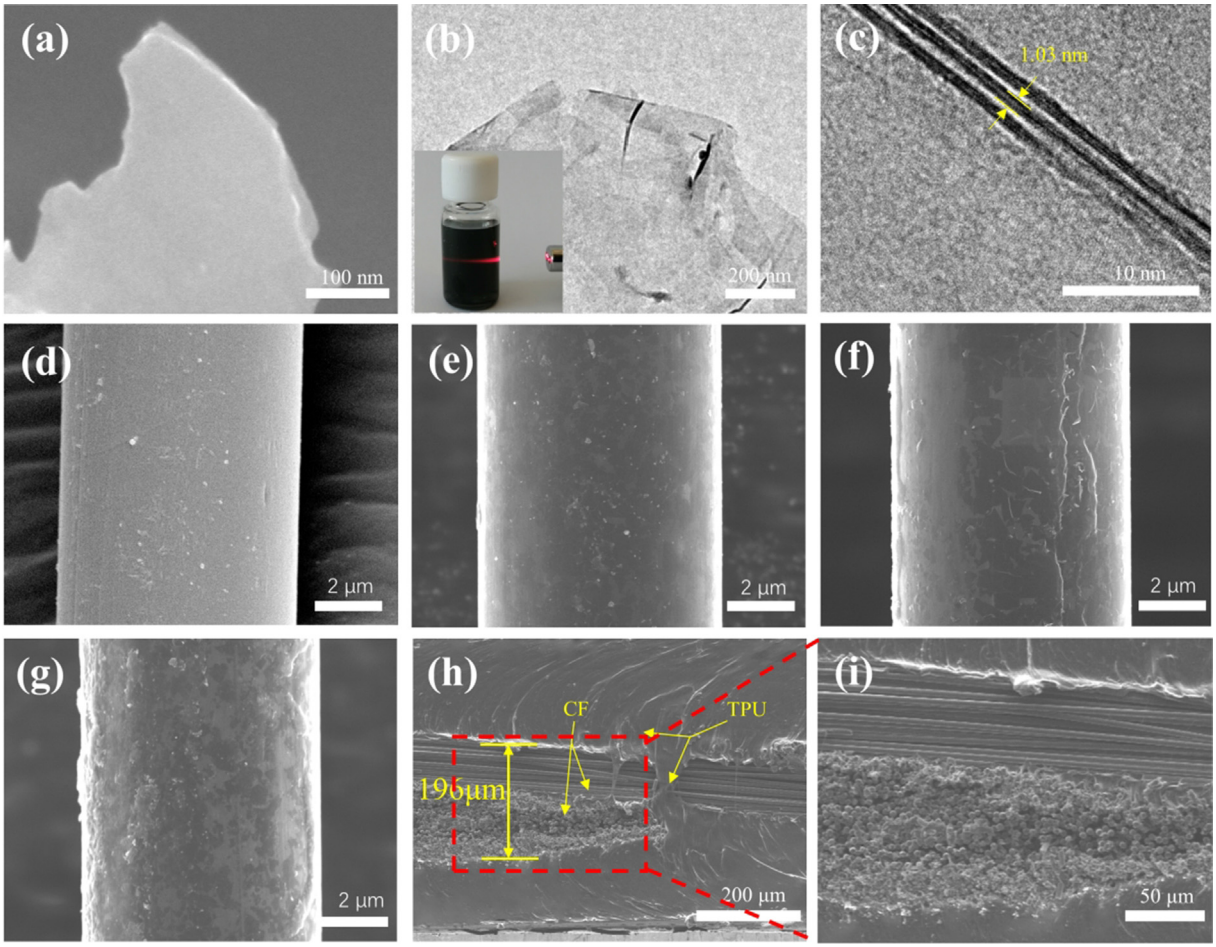

Fig. 2. (a) SEM images of $Ti_3C_2T_x$ MXene; (b-c) TEM of $Ti_3C_2T_x$ MXene; SEM images of (d-g) CF coated with different $Ti_3C_2T_x$ MXene mass fractions; (h-i) Cross-sectional views of the $Ti_3C_2T_x$ MXene/CFf/TPU composite.

Table 1
Constant values of permeability formula.

Fiber arrangement	C_1	$V_{f,max}$
Quadratic	$C_1 = \frac{16}{9\pi\sqrt{2}}$	$\frac{\pi}{4}$
Hexagonal	$C_1 = \frac{16}{9\pi\sqrt{6}}$	$\frac{\pi}{2\sqrt{3}}$

and 533.0 eV correspond to TiO_2, C—Ti—O_x, C—Ti—$(OH)_x$ and H_2O, respectively [22,30]. As shown in Table S1, compared with pure MXene, the elemental composition of MXene/CFf nanocomposites changes significantly. The ratio of the C/Ti atom content in pure MXene is 1.01, and the ratio of the C/Ti atom content in MXene/CFf is 13.97. The results showed that the ratio of the organic components increased [29]. As shown in Table S2, the binding energies of Ti-C ($2p_{3/2}$), Ti (II) ($2p_{3/2}$), Ti-C ($2p_{1/2}$) and Ti (II) ($2p_{1/2}$) were significantly improved by the introduction of CF. As shown in Table S3, when MXene was introduced into CF, the atomic percentage of C-Ti-O_x increased, indicating an interaction between the MXene layer and CF fabric. In addition, according to the analysis of the Ti spectrum, the existence of a small amount of TiO_2 indicates that local oxidation occurred during the preparation of $Ti_3C_2T_x$ MXene. However, it is worth noting that this has a negligible effect on the experimental results, and similar results have been reported in other studies [13,31]. Thus, it can be concluded that the $Ti_3C_2T_x$ MXene molecules were deposited on the surface of the CF fabric [32].

3.3. Mechanical performance

Fig. 4a–b shows the tensile stress–strain curves and tensile strength of the $Ti_3C_2T_x$ MXene/CFf/TPU composites. The tensile strength of the CFf/TPU composite can reach 68.6 MPa, suggesting a relatively low strength. With the $Ti_3C_2T_x$ MXene mass fraction increasing from 0.32% to 1.06%, the value of the tensile strength increases from 96.3 MPa to 170.2 MPa, indicating that the introduction of $Ti_3C_2T_x$ MXene can improve the tensile strength of the $Ti_3C_2T_x$ MXene/CFf/TPU composite. Fig. 4c shows a comparison of the tensile strengths of $Ti_3C_2T_x$ MXene/CFf/TPU composites and other composites in previous studies. The tensile strength of the $Ti_3C_2T_x$ MXene/CFf/TPU-3 composite is greater than that of many other composites. The details are provided in Table S4 in the Supporting Information. Many existing composites have the characteristics of high density and low tensile strength. However, the $Ti_3C_2T_x$ MXene/CFf/TPU composite shows high tensile properties (170.2 MPa) and relatively low density (1.25 g/cm^3). This means that the $Ti_3C_2T_x$ MXene/CFf/TPU composites have excellent mechanical properties, which can satisfy applications where outstanding mechanical performance is required. Furthermore, folding tests were conducted to demonstrate the excellent flexibility of the composites. As shown in Fig. 4d–e, it is apparent that the composite can be easily folded at a large angle. The bending and twisting processes of the $Ti_3C_2T_x$ MXene/CFf/TPU-3 composite are shown in Video S1. After many folding-releasing operations, the composite could easily return to its original shape. The surface of the compos-

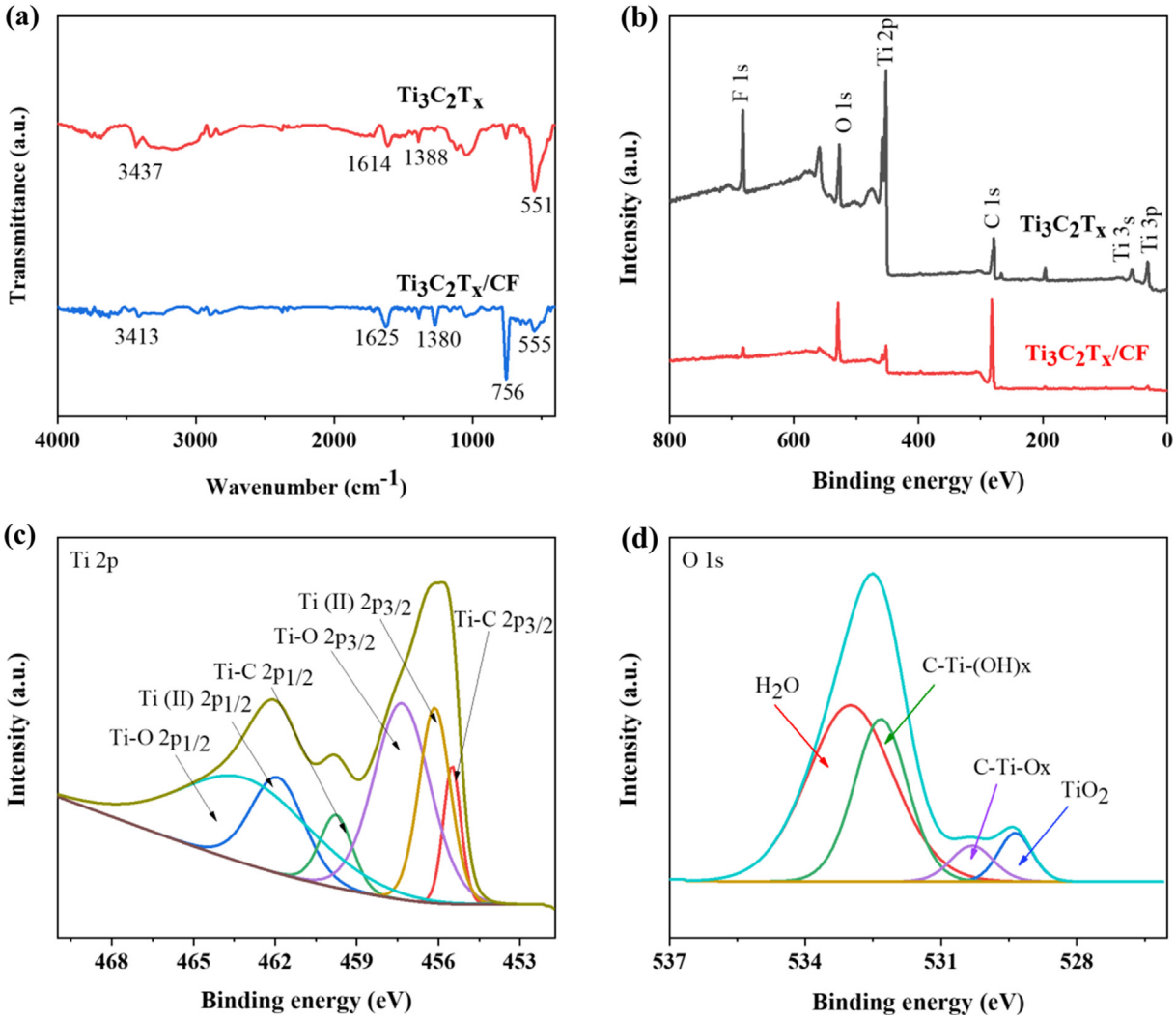

Fig. 3. (a) FTIR and (b) XPS spectra of $Ti_3C_2T_x$ and $Ti_3C_2T_x$ MXene/CF nanocomposite; (c) Ti 2p XPS spectrum of $Ti_3C_2T_x$ MXene/CF nanocomposite; (d) O 1s XPS spectrum of $Ti_3C_2T_x$ MXene/CF nanocomposite.

ite remained in good condition, without wrinkles and cracks, which proves that the composite has exceptional flexibility. Fig. 4f and Video S2 show the image of the $Ti_3C_2T_x$ MXene/CFf/TPU-3 composite holding up a 5 kg iron block, indicating that the composite has a large load-bearing capacity. As shown in Fig. 4g, the interlaminar shear strength of CFf/TPU, MXene/CFf/TPU-1, MXene/CFf/TPU-2 and MXene/CFf/TPU-3 composites are 35.76 MPa, 42.54 MPa, 51.86 MPa and 56.71 MPa, respectively. Compared with the CFf/TPU composite, the interlaminar shear strength of the MXene/CFf/TPU-3 composite increased by 58.6%. In addition, as shown in Fig. 2g, MXene nanosheets were observed on the CF surface. Therefore, it can be inferred that the presence of MXene significantly improved the bonding strength of the interface.

Fig. 4h shows the interface strengthening mechanism of the composites. First, the surface of the treated CF fabric has many active functional groups (—COOH), and there are abundant functional groups (—OH) on the surface of $Ti_3C_2T_x$ MXene, which can interact with each other to form new chemical bonds. The polymer increases the chemical bond between the CF fabric and matrix, thereby increasing the interface strength [33]. In addition, the existence of mechanical interlocking has an important effect on the improvement of the tensile strength of the $Ti_3C_2T_x$ MXene/CFf/TPU composite [34,35]. When the $Ti_3C_2T_x$ MXene molecules are deposited on the surface of the CF, TPU molecules can enter the space between the $Ti_3C_2T_x$ MXene and the CF, which facilitates the mechanical interlocking of the interface. As shown in Fig. 2d–g, the surface of the untreated CF is relatively smooth, but the CF surface of the CF becomes rough after $Ti_3C_2T_x$ MXene treatment. The increase of the internal contact area of the composite improves the adsorption of TPU, which is conducive to the mechanical interlocking effect of the CF surface. In addition, the van der Waals forces between molecules are beneficial for improving the bonding performance of the interface [36]. Therefore, the mechanical performance of $Ti_3C_2T_x$ MXene/CFf/TPU composite improves with increasing $Ti_3C_2T_x$ MXene content (0.32 wt% to 1.06 wt%). However, because the interface interaction of CF/TPU composite was poor, the mechanical performance was lower than that of the $Ti_3C_2T_x$ MXene/CFf/TPU composite.

For layered $Ti_3C_2T_x$ MXene/CFf/TPU composites, there are three main damage modes: matrix cracking, interface debonding slip, and fiber breakage. The mesoscopic damage modes of the $Ti_3C_2T_x$ MXene/CFf/TPU composite were analyzed. Fig. 5a shows the interface debonding slip phenomenon of the composite. Interface debonding is an important damage mode in composites. Some CF tows were debonded from the TPU. As microcracks are transmitted

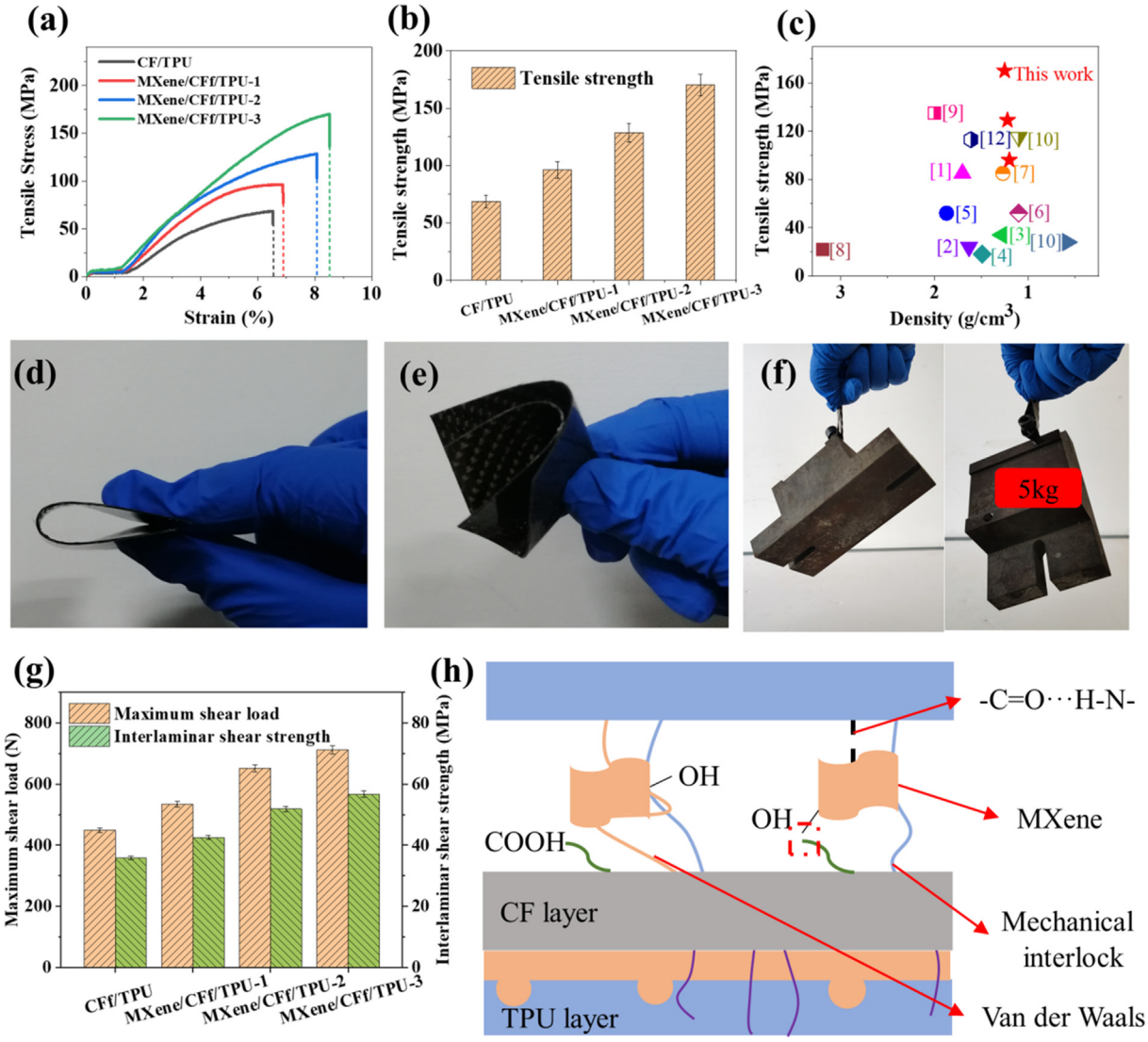

Fig. 4. (a) Tensile stress–strain curves of the $Ti_3C_2T_x$ MXene/CFf/TPU composites; (b) Tensile strength of the $Ti_3C_2T_x$ MXene/CFf/TPU composites; (c) Comparison of the tensile strength of the $Ti_3C_2T_x$ MXene/CFf/TPU composites and other composites in other previous studies. The numbers in (c) are the sample numbers in Table S4 in the Supporting Information; (d-e) Bending and twisting processes of composites; (f) Photograph of the $Ti_3C_2T_x$ MXene/CFf/TPU-3 composite supporting the weight of a 5 kg iron block; (g) The interlaminar shear strength of CFf/TPU and $Ti_3C_2T_x$ MXene/CFf/TPU composite; (h)The interface strengthening mechanism of the $Ti_3C_2T_x$ MXene/CFf/TPU composites.

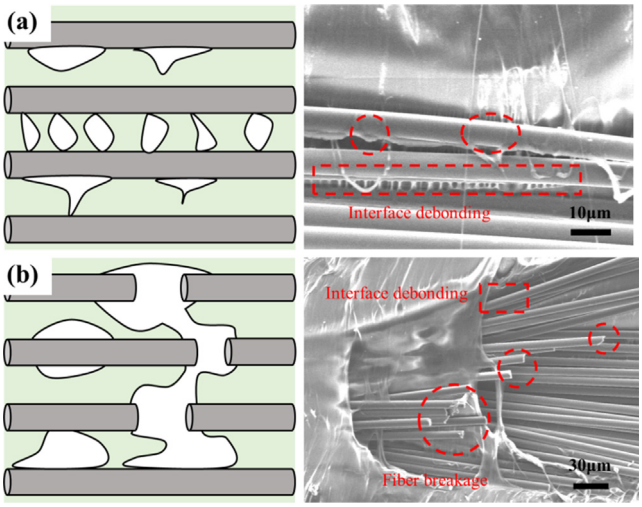

Fig. 5. Damage mode of MXene/CFf/TPU composite: (a) Interface debonding; (b) Fiber breakage.

inside the composite, when they encounter the interface, the microcracks can be deflected and thus spread along the interface over a large area because of possible micro-defects at the interface, resulting in an interfacial debonding slip of carbon fibers [37]. Fig. 5b shows the fracture of the fibers inside the composite. As we know, fibers are the main load-bearing unit of $Ti_3C_2T_x$ MXene/CFf/TPU composite. When a large stress is applied, the local fiber breaks owing to severe stress concentration [38]. When the stress is high, interface debonding and fiber breakage can coexist.

The synergistic strengthening and interfacial enhancement mechanism of the $Ti_3C_2T_x$ MXene/CFf/TPU composite were also investigated. As shown in Fig. 6a, MXene molecules are connected to CF by van der Waals forces, which gradually fail when the tensile force increases. As shown in Fig. 6b, some MXene molecules were connected to CF by van der Waals forces and covalent bonds. The strength of the van der Waals force is less than that of the covalent bond; therefore, the van der Waals forces gradually fail when the tensile force increases. When the tensile force increased further, the covalent bonds gradually break. In addition, the presence of covalent bonds may impose geometric constraints on the motion

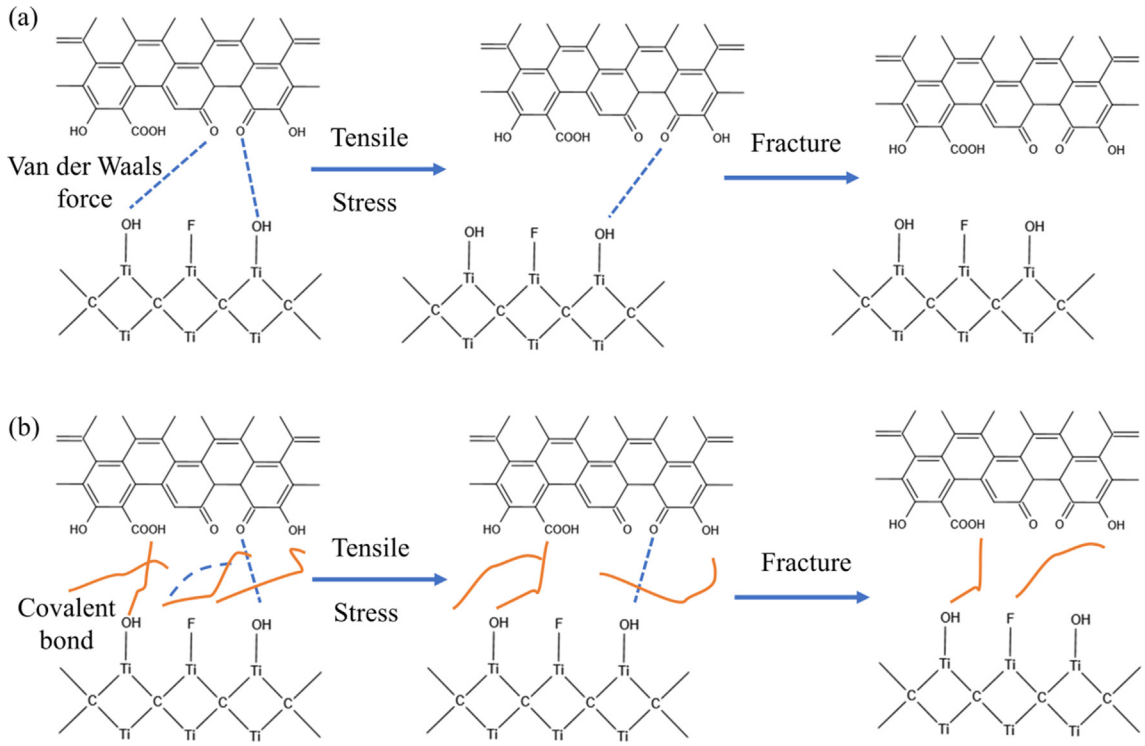

Fig. 6. Schematic diagram of the fracture mechanism of MXene/CFf/TPU composite.

of independent polymer chains, which further leads to the nanoconfinement effect [39]. Therefore, the synergistic strengthening effect of van der Waals forces and covalent bonds enhances the strength of the composite.

3.4. EMI shielding performance and electrical property

The EMI shielding performances of the TPU, CFf/TPU, $Ti_3C_2T_x$ MXene/CFf/TPU-1, $Ti_3C_2T_x$ MXene/CFf/TPU-2 and $Ti_3C_2T_x$ MXene/

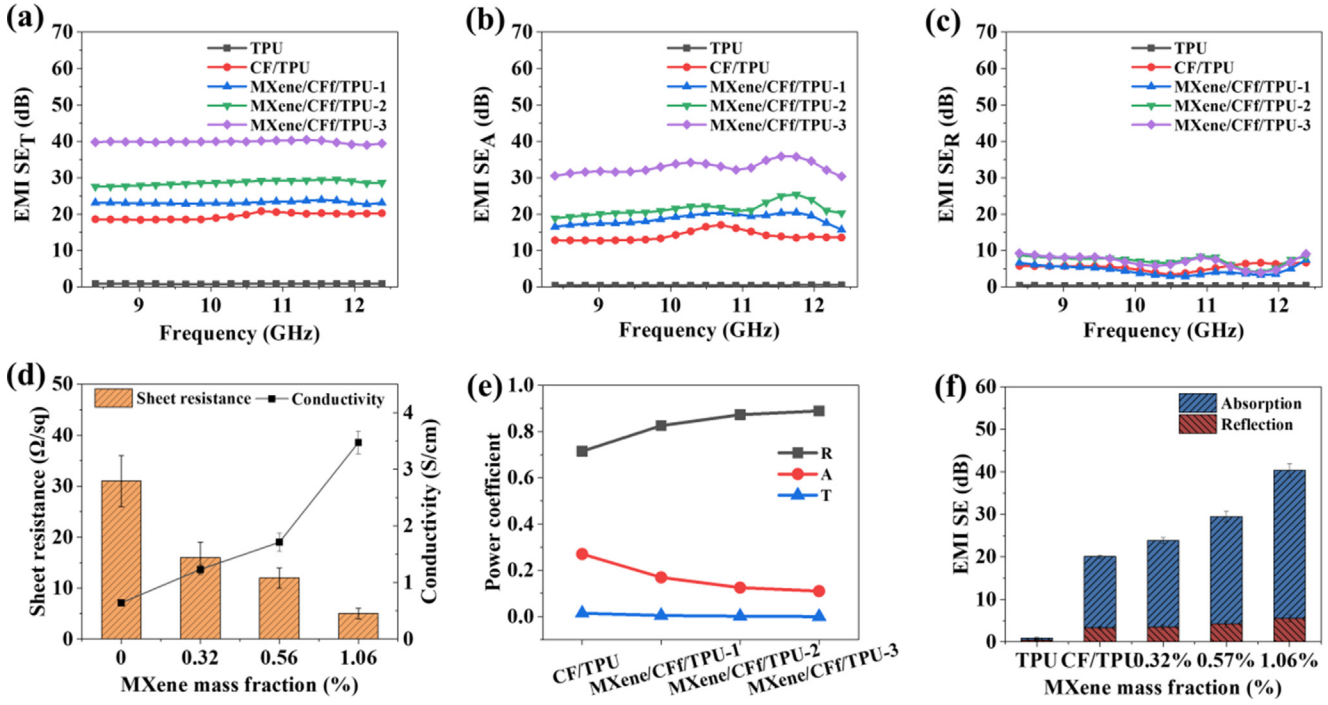

Fig. 7. EMI-SE of (a) SE_T, (b) SE_A and (c) SE_R; (d) Sheet resistance and conductivity of $Ti_3C_2T_x$ MXene/CFf/TPU composites; (e) Power coefficient of $Ti_3C_2T_x$ MXene/CFf/TPU composites; (f) SE at various EMI shielding mechanism (% absorption and % reflection) for different $Ti_3C_2T_x$ MXene loading.

CFf/TPU-3 composites are shown in Fig. 7a. The TPU has a small SE_T value, which means that the TPU has little effect on the dissipation of electromagnetic waves. The CFf/TPU composite had relatively poor EMI shielding properties, with the SE_T value reaching 20.8 dB. When the $Ti_3C_2T_x$ MXene content increased, the EMI-SE of the $Ti_3C_2T_x$ MXene/CFf/TPU composites increased significantly. For a $Ti_3C_2T_x$ MXene content of 0.32%, the SE_T, SE_A and SE_R of $Ti_3C_2T_x$ MXene/CFf/TPU-1 composite were 23.9 dB, 20.4 dB and 3.5 dB, respectively. As the $Ti_3C_2T_x$ MXene content increased from 0.32% to 0.57%, the SE_T, SE_A and SE_R of the $Ti_3C_2T_x$ MXene/CFf/TPU-2 composite exhibited a rising trend of 29.5 dB, 25.3 dB and 4.2 dB, respectively. When the $Ti_3C_2T_x$ MXene content increased to 1.06%, the SE_T, SE_A and SE_R of the $Ti_3C_2T_x$ MXene/CFf/TPU-3 composite were 40.4 dB, 34.8 dB and 5.6 dB, respectively. The results show that the increase of $Ti_3C_2T_x$ MXene significantly improved the EMI shielding properties of the $Ti_3C_2T_x$ MXene/CFf/TPU composite. Besides, the SE_A and SE_R of the composites were also measured, as shown in Fig. 7b–c. The SE_A value was much higher than the SE_R value. For instance, the SE_A of the $Ti_3C_2T_x$ MXene/CFf/TPU-3 composite was 34.8 dB and the SE_R was 5.6 dB, which means that SE_A accounts for more than 80% in SE_T. Fig. 7d shows the average sheet resistance and conductivity of the $Ti_3C_2T_x$ MXene/CFf/TPU composites. The sheet resistance of $Ti_3C_2T_x$ MXene/CFf/TPU-1 was 16 Ω/sq. With the increase of $Ti_3C_2T_x$ MXene content, this value gradually decreases. The sheet resistance of $Ti_3C_2T_x$ MXene/CFf/TPU-2 was 12 Ω/sq and the sheet resistance of $Ti_3C_2T_x$ MXene/CFf/TPU-3 was 5 Ω/sq. The conductivity of $Ti_3C_2T_x$ MXene/CFf/TPU-1, $Ti_3C_2T_x$ MXene/CFf/TPU-2 and $Ti_3C_2T_x$ MXene/CFf/TPU-3 composites were 1.23 S/cm, 1.71 S/cm, 3.47 S/cm, respectively. This may be due to the increase of $Ti_3C_2T_x$ MXene content, which makes the conductive network in the composite more complex.

In addition, to evaluate the ability of the composite to absorb, reflect, and transmit electromagnetic waves, the power coefficients of absorption (A), reflection (R) and transmission (T) were measured. As shown in Fig. 7e, when the content of MXene increased, the value of R increased, while A and T decreased. R is always much higher than A, and A is always higher than T. This can be attributed to the fact that when electromagnetic waves are directed towards the composite, the reflection of EM waves always has priority over absorption. And the mismatch between the external free space and the composite impedance leads to more reflections, so the value of R is always greater than A. This indicates that the shielding mechanism of the $Ti_3C_2T_x$ MXene/CFf/TPU EMI shielding composite was determined by reflection. The the remaining part of the electromagnetic waves that penetrate into the interior of the composite will be absorbed and reflected. In terms of the electromagnetic waves inside the composites, A_{eff} is usually used to evaluate the potential of the composites to absorb electromagnetic waves. As shown in Fig. S2, the value of A_{eff} is greater than 0.95, which means that more than 95% of the power is absorbed. As shown in Fig. 7f, the value of SE_A is much higher than that of SE_R. Besides, with the increase of MXene content, the increase of SE_T and SE_A is obvious, but the increase of SE_R is slow, which means that the increase of SE_T is mainly attributed to the increase of SE_A. For example, as the $Ti_3C_2T_x$ MXene mass fraction increases from 0.56% to 1.06%, the SE_A of the $Ti_3C_2T_x$ MXene/CFf/TPU composite increases from 25.3 dB to 34.8 dB, but the SE_R value increases from 4.2 dB to 5.6 dB. The lower SE_R and larger SE_A indicate that the attenuation of electromagnetic waves that penetrate into the composite is dominated by absorption [22].

Fig. 8 shows the EMI shielding mechanism of the $Ti_3C_2T_x$ MXene/CFf/TPU composite. When the EM waves radiate into the composite, there will be a large impedance mismatch between the external free space and the composite, and part of the EM waves are reflected on the surface of the $Ti_3C_2T_x$ MXene/CFf/TPU composite, and the rest of the EM waves enter the composite. First, the incident electromagnetic waves propagate in the TPU layer. Because the EMI-SE value of TPU is very small, the electromagnetic waves dissipate little in the TPU layer. The electromagnetic waves then propagate from the TPU to the CF fabric-coated $Ti_3C_2T_x$ MXene. The unique layered structure of $Ti_3C_2T_x$ MXene and the composite can expand the propagation path of electromagnetic waves. As a result, the incident electromagnetic waves can undergo multiple reflections or scattering processes during which much of the electromagnetic waves are absorbed. Besides, when the content of $Ti_3C_2T_x$ MXene increases, more interfaces are formed, thus improving the absorption of electromagnetic waves. When electromagnetic waves pass through the MXene layer and CFf layer, the movement of charge carriers will produce micro current [40]. In the process of movement, an anti-magnetic field can be generated to offset the initial interference magnetic field. Moreover, these charge carriers will produce heat loss during motion, which means that some EM waves dissipate in the form of thermal energy. In addition, the free carriers in the media will gradually accumulate at the interface of different media, such as those between $Ti_3C_2T_x$ MXene, CF and TPU. This may lead to an uneven distribution of charge on the interface of different media, further contributing to the electric dipole moment and causing polarization of the interface [42,43]. The interface polarization that exists in the composites can be conducive to further absorption of electromagnetic waves [15,43]. When the incident electromagnetic wave dissipates in the CF layer, the remaining part of the incident EM wave propagates from the CF layer to the TPU layer on the other side. Again, the remaining portion of the incident electromagnetic waves can be absorbed and reflected in the CF layer. Finally, after multiple absorption and reflection processes, only a small portion of the electromagnetic waves can pass through the composite directly, which indicates that the $Ti_3C_2T_x$ MXene/CFf/TPU composite has remarkable electromagnetic shielding performance.

In practical applications, EMI shielding materials usually require higher mechanical properties. For example, some mobile phone manufacturers (Samsung, Huawei, etc.) have released several folding smartphones, which require not only excellent mechanical properties, but also good stability and cycle durability of the composite. Therefore, the stability of the $Ti_3C_2T_x$ MXene/CFf/TPU composite was analyzed. Taking the $Ti_3C_2T_x$ MXene/CFf/TPU-2 composite as an example, Fig. 9a shows the bending and releasing operation of the $Ti_3C_2T_x$ MXene/CFf/TPU-2 composite. Fig. 9b illustrates the variation of the relative resistance of the $Ti_3C_2T_x$ MXene/CFf/TPU-2 composite. The relative resistance (R/R_0) value of the composite changed slightly within the range of 0.96 to 1. After 1000 bending-releasing operations, the R/R_0 value was 0.99. Even after 2000 bending-releasing operations, the R/R_0 value was 0.98, still maintaining a large value. The results indicate that the resistance of the composite can still maintain good resistance stability even after multiple bending-releasing operations. As shown in Fig. 9c, the EMI shielding performance of the $Ti_3C_2T_x$ MXene/CFf/TPU-2 composite after multiple bending-releasing operations was also measured. The EMI shielding value of the $Ti_3C_2T_x$ MXene/CFf/TPU-2 composite did not decrease significantly with the increase of the number of bending-releasing operations. After 4000 folding-releasing operations, the composite can still maintain an EMI-SE of 25.9 dB. The results showed that the composite exhibited excellent resistance stability and EMI stability. To further explore the properties of the composite, an index of EMI-SE/Thickness (SE/t) was proposed [13]. Fig. 9d and Table S5 show that the SE/t value of $Ti_3C_2T_x$ MXene/CFf/TPU composite can reach 80.8 dB/mm, which is competitive compared to other materials. Besides, as shown in Table S6 and Fig. S3, compared with other materials, although the performance of $Ti_3C_2T_x$/CFf/TPU composite is not the best, it is still very competitive. Fig. 9e shows the com-

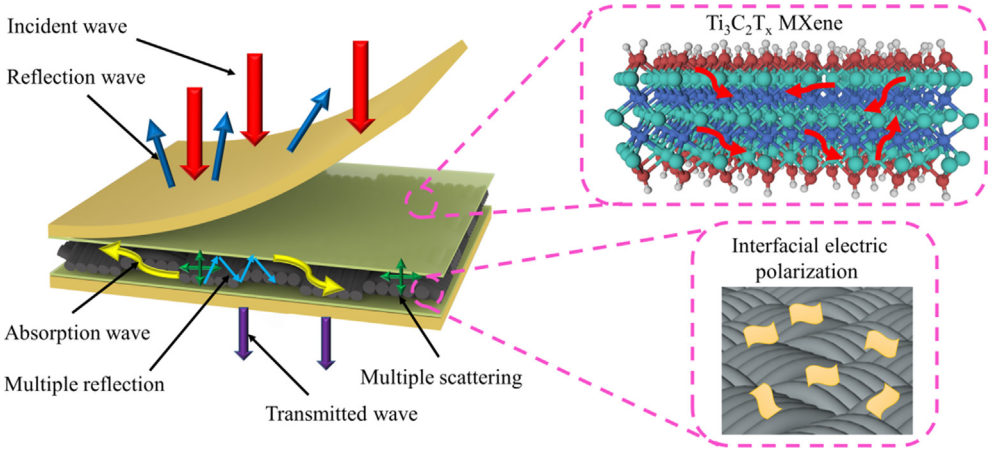

Fig. 8. Schematic diagram of EMI shielding mechanism of $Ti_3C_2T_x$ MXene/CFf/TPU composite.

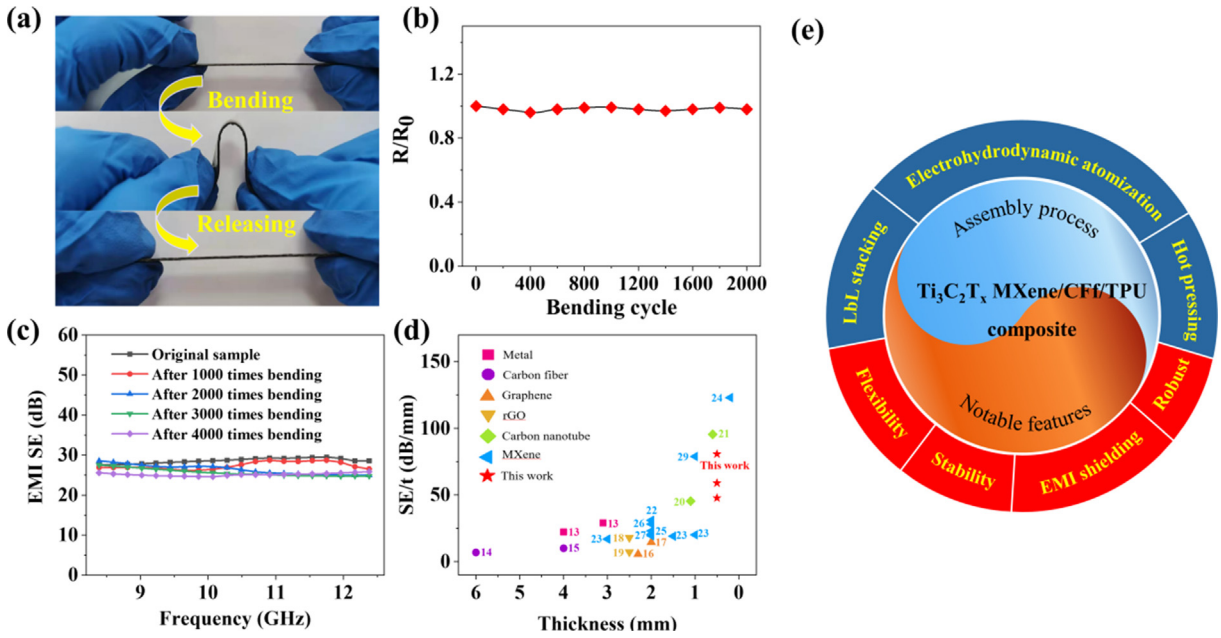

Fig. 9. (a) Bending and releasing operation of $Ti_3C_2T_x$ MXene/CFf/TPU-2 composite; (b) Relative resistance (R/R_0) value of $Ti_3C_2T_x$ MXene/CFf/TPU-2 composite; (c) EMI shielding performance of $Ti_3C_2T_x$ MXene/CFf/TPU-2 after multiple times bending; (d) Comparison of EMI shielding performance of $Ti_3C_2T_x$ MXene/CFf/TPU with other reported materials, and the number in (d) are reference numbers listed in Table S5 in the Supporting Information; (e) Comprehensive performance of $Ti_3C_2T_x$ MXene/CFf/TPU composite.

prehensive performance of the $Ti_3C_2T_x$ MXene/CFf/TPU composite, such as flexibility, stability, outstanding EMI properties and mechanical properties. These superior properties enable the unique $Ti_3C_2T_x$ MXene/CFf/TPU composite broad application prospects in many areas where lightweight, high mechanical and EMI shielding properties are needed.

4. Conclusion

In this work, the $Ti_3C_2T_x$ MXene/CFf/TPU composite was fabricated by EHDA deposition, hot pressing and layer-by-layer stacking technology. By changing the number of the spray-drying cycles, the CF fabric with $Ti_3C_2T_x$ MXene loadings of 0.32 ~ 1.06 wt% was obtained. As the content of $Ti_3C_2T_x$ MXene increased, the tensile strength of the composite increased, reaching a maximum of 170.2 MPa. This can be attributed to the existence of $Ti_3C_2T_x$ MXene, which improves the mechanical interlock between CF fabric and TPU. From the analysis, it can be concluded that interfacial debonding and fiber breakage are the main damage modes of the composites. Furthermore, the fabricated $Ti_3C_2T_x$ MXene/CFf/TPU-3 composite exhibited an EMI-SE of 40.4 dB at a thickness of 0.5 mm when the $Ti_3C_2T_x$ MXene mass fraction was 1.06%. As the MXene content increased, the EMI shielding efficiency gradually increased, corresponding to the change in electrical conductivity. Moreover, the composite retained excellent resistance stability, EMI-SE stability and flexibility even after multiple bending and releasing cycles. In summary, the $Ti_3C_2T_x$ MXene/CFf/TPU composite not only has outstanding EMI shielding properties, but also possesses excellent mechanical properties, which may have broad application prospects in intelligent wear, wireless communication electronic equipment and other fields.

CRediT authorship contribution statement

Ningmin Duan: Conceptualization, Data curation, Formal analysis, Investigation, Methodology, Software, Writing – original draft.

Zhenyu Shi: Conceptualization, Formal analysis, Funding acquisition, Resources, Methodology, Supervision, Validation, Writing – review & editing. **Zhaohui Wang:** Investigation, Software, Supervision, Validation. **Bin Zou:** Supervision, Validation. **Chengpeng Zhang:** Conceptualization, Resources, Methodology. **Jilai Wang:** Investigation, Supervision, Validation. **Jianren Xi:** Investigation, Conceptualization, Methodology. **Xiaoshuai Zhang:** Project administration. **Xianzhi Zhang:** Formal analysis, Writing – review & editing. **Guilong Wang:** Conceptualization, Formal analysis, Resources, Methodology, Supervision, Validation, Writing – review & editing.

Declaration of Competing Interest

The authors declare that they have no known competing financial interests or personal relationships that could have appeared to influence the work reported in this paper.

Acknowledgments

This work is financially supported by the National Natural Science Foundation of China (51975334 and U21A20134), Key R&D project of Shandong Province (2019JMRH0407).

Appendix A. Supplementary material

Supplementary data to this article can be found online at https://doi.org/10.1016/j.matdes.2022.110382.

References

[1] X. Zheng, W. Nie, Q. Hu, X. Wang, Z. Wang, L. Zou, X. Hong, H. Yang, J. Shen, C. Li, Multifunctional RGO/$Ti_3C_2T_x$ MXene fabrics for electrochemical energy storage, electromagnetic interference shielding, electrothermal and human motion detection, Mater. Des. 200 (2021) 109442.
[2] L. Xu, Y. Xiong, B. Dang, Z. Ye, C. Jin, Q. Sun, X. Yu, In-situ anchoring of Fe3O4/ZIF-67 dodecahedrons in highly compressible wood aerogel with excellent microwave absorption properties, Mater. Des. 182 (2019) 108006.
[3] T. Guo, X. Chen, L. Su, C. Li, X. Huang, X.Z. Tang, Stretched graphene nanosheets formed the "obstacle walls" in melamine sponge towards effective electromagnetic interference shielding applications, Mater. Des. 182 (2019) 108029.
[4] X. Mei, L. Lu, Y. Xie, W. Wang, Y. Tang, K.S. Teh, An ultra-thin carbon-fabric/graphene/poly(vinylidene fluoride) film for enhanced electromagnetic interference shielding, Nanoscale. 11 (28) (2019) 13587–13599.
[5] Y. Wang, Z. Fan, H. Zhang, J. Guo, D. Yan, S. Wang, K. Dai, Z. Li, 3D-printing of segregated carbon nanotube / polylactic acid composite with enhanced electromagnetic interference shielding and mechanical performance, Mater. Des. 197 (2021) 109222.
[6] J. Chen, Z. Zhu, H. Zhang, S. Tian, S. Fu, Wood-derived nanostructured hybrid for efficient flame retarding and electromagnetic shielding, Mater. Des. 204 (2021) 109695.
[7] Y. Zhang, W. Cheng, W. Tian, J. Lu, L. Song, K.M. Liew, B. Wang, Y. Hu, Nacre-Inspired Tunable Electromagnetic Interference Shielding Sandwich Films with Superior Mechanical and Fire-Resistant Protective Performance, ACS Appl. Mater. Interfaces. 12 (5) (2020) 6371–6382.
[8] Z. Ma, S. Kang, J. Ma, L. Shao, Y. Zhang, C. Liu, A. Wei, X. Xiang, L. Wei, J. Gu, Ultraflexible and Mechanically Strong Double-Layered Aramid Nanofiber-$Ti_3C_2T_x$ MXene/Silver Nanowire Nanocomposite Papers for High-Performance Electromagnetic Interference Shielding, ACS Nano. 14 (7) (2020) 8368–8382.
[9] S. Zhao, Y. Yan, A. Gao, S. Zhao, J. Cui, G. Zhang, Flexible Polydimethylsilane Nanocomposites Enhanced with a Three-Dimensional Graphene/Carbon Nanotube Bicontinuous Framework for High-Performance Electromagnetic Interference Shielding, ACS Appl. Mater. Interfaces. 10 (31) (2018) 26723–26732.
[10] Z. Chen, C. Xu, C. Ma, W. Ren, H.-M. Cheng, Lightweight and flexible graphene foam composites for high-performance electromagnetic interference shielding, Adv. Mater. 25 (9) (2013) 1296–1300.
[11] H. Lu, Z. Li, X. Qi, L. Xu, Z. Chi, D. Duan, M.Z. Islam, W. Wang, X. Jin, Y. Zhu, Y. Fu, L. Cui, Y. Zhuang, Y. Dong, Flexible, electrothermal-driven controllable carbon fiber/poly(ethylene-co-vinyl acetate) shape memory composites for electromagnetic shielding, Compos. Sci. Technol. 207 (2021) 108697.
[12] Z. Ma, S. Kang, J. Ma, L. Shao, A. Wei, C. Liang, J. Gu, B. Yang, D. Dong, L. Wei, Z. Ji, High-Performance and Rapid-Response Electrical Heaters Based on Ultraflexible, Heat-Resistant, and Mechanically Strong Aramid Nanofiber/Ag Nanowire Nanocomposite Papers, ACS Nano. 13 (7) (2019) 7578–7590.
[13] D. Hu, X. Huang, S. Li, P. Jiang, Flexible and durable cellulose/MXene nanocomposite paper for efficient electromagnetic interference shielding, Compos. Sci. Technol. 188 (2020) 107995.
[14] Y. Gogotsi, B. Anasori, The Rise of MXenes, ACS Nano. 13 (8) (2019) 8491–8494.
[15] Q. Zhou, K. Qian, J. Fang, M. Miao, S. Cao, X. Feng, UV-light modulated $Ti_3C_2T_x$ MXene/g-C_3N_4 heterojunction film for electromagnetic interference shielding, Compos. Part A Appl. Sci. Manuf. 134 (2020) 105899.
[16] F. Shahzad, M. Alhabeb, C.B. Hatter, B. Anasori, S. Man Hong, C.M. Koo, Y. Gogotsi, Electromagnetic interference shielding with 2D transition metal carbides (MXenes), Science 353 (6304) (2016) 1137–1140.
[17] X. Jin, J. Wang, L. Dai, X. Liu, L. Li, Y. Yang, Y. Cao, W. Wang, H. Wu, S. Guo, Flame-retardant poly(vinyl alcohol)/MXene multilayered films with outstanding electromagnetic interference shielding and thermal conductive performances, Chem. Eng. J. 380 (2020) 122475.
[18] J.Q. Luo, S. Zhao, H. Bin Zhang, Z. Deng, L. Li, Z.Z. Yu, Flexible, stretchable and electrically conductive MXene/natural rubber nanocomposite films for efficient electromagnetic interference shielding, Compos. Sci. Technol. 182 (2019) 107754.
[19] H. Wei, M. Wang, W. Zheng, Z. Jiang, Y. Huang, 2D $Ti_3C_2T_x$ MXene/aramid nanofibers composite films prepared via a simple filtration method with excellent mechanical and electromagnetic interference shielding properties, Ceram. Int. 46 (5) (2020) 6199–6204.
[20] S. Park, S.W. Heo, W. Lee, D. Inoue, Z. Jiang, K. Yu, H. Jinno, D. Hashizume, M. Sekino, T. Yokota, K. Fukuda, K. Tajima, T. Someya, Self-powered ultra-flexible electronics via nano-grating-patterned organic photovoltaics, Nature 561 (7724) (2018) 516–521.
[21] B. Nie, R. Huang, T. Yao, Y. Zhang, Y. Miao, C. Liu, J. Liu, X. Chen, Textile-Based Wireless Pressure Sensor Array for Human-Interactive Sensing, Adv. Funct. Mater. 29 (2019) 1808786.
[22] Z. Fan, D. Wang, Y. Yuan, Y. Wang, Z. Cheng, Y. Liu, Z. Xie, A lightweight and conductive MXene/graphene hybrid foam for superior electromagnetic interference shielding, Chem. Eng. J. 381 (2020) 122696.
[23] C. Liang, H. Qiu, P. Song, X. Shi, J. Kong, J. Gu, Ultra-light MXene aerogel/wood-derived porous carbon composites with wall-like "mortar/brick" structures for electromagnetic interference shielding, Sci. Bull. 65 (8) (2020) 616–622.
[24] X. Li, J. Deng, L. Liu, R. Duan, D. Ge, Fabrication of WS_2/C composite coatings via electrohydrodynamic atomization and their tribology behaviours, Appl. Surf. Sci. 538 (2021) 148128.
[25] Z. Wang, Q. Wang, B. Li, Y. Zhang, J. Wang, J. Tu, An experimental investigation on cone-jet mode in electrohydrodynamic (EHD) atomization, Exp. Therm. Fluid Sci. 114 (2020) 110054.
[26] Z. Zong, F. Ren, Z. Guo, Z. Lu, Y. Jin, Y. Zhao, P. Ren, Dual-functional carbonized loofah@GNSs-CNTs reinforced by cyanate ester composite with highly efficient electromagnetic interference shielding and thermal management, Compos. Part B Eng. 223 (2021) 109132.
[27] E. Syerko, C. Binetruy, S. Comas-Cardona, A. Leygue, A numerical approach to design dual-scale porosity composite reinforcements with enhanced permeability, Mater. Des. 131 (2017) 307–322.
[28] M.W. Tahir, F. Stig, M. Åkermo, S. Hallström, A numerical study of the influence from architecture on the permeability of 3D-woven fibre reinforcement, Compos. Part A Appl. Sci. Manuf. 74 (2015) 18–25.
[29] W. Yang, J.J. Liu, L.L. Wang, W. Wang, A.C.Y. Yuen, S. Peng, B. Yu, H.D. Lu, G.H. Yeoh, C.H. Wang, Multifunctional MXene/natural rubber composite films with exceptional flexibility and durability, Compos. Part B Eng. 188 (2020) 107875.
[30] J. Yan, C.E. Ren, K. Maleski, C.B. Hatter, B. Anasori, P. Urbankowski, A. Sarycheva, Y. Gogotsi, Flexible MXene/Graphene Films for Ultrafast Supercapacitors with Outstanding Volumetric Capacitance, Adv. Funct. Mater. 27 (2017) 1701264.
[31] K. Rajavel, S. Luo, Y. Wan, X. Yu, Y. Hu, P. Zhu, R. Sun, C. Wong, 2D $Ti_3C_2T_x$ MXene/polyvinylidene fluoride (PVDF) nanocomposites for attenuation of electromagnetic radiation with excellent heat dissipation, Compos. Part A Appl. Sci. Manuf. 129 (2020) 105693.
[32] X. Zhang, X. Wang, Z. Lei, L. Wang, M. Tian, S. Zhu, H. Xiao, X. Tang, L. Qu, Flexible MXene-Decorated Fabric with Interwoven Conductive Networks for Integrated Joule Heating, Electromagnetic Interference Shielding, and Strain Sensing Performances, ACS Appl. Mater. Interfaces 12 (12) (2020) 14459–14467.
[33] Y. Fu, H. Li, W. Cao, Enhancing the interfacial properties of high-modulus carbon fiber reinforced polymer matrix composites via electrochemical surface oxidation and grafting, Compos. Part A Appl. Sci. Manuf. 130 (2020) 105719.
[34] T. Sun, M. Li, S. Zhou, M. Liang, Y. Chen, H. Zou, Multi-scale structure construction of carbon fiber surface by electrophoretic deposition and electropolymerization to enhance the interfacial strength of epoxy resin composites, Appl. Surf. Sci. 499 (2020) 143929.
[35] J. Lin, P. Xu, L. Wang, Y. Sun, X. Ge, G. Li, X. Yang, Multi-scale interphase construction of self-assembly naphthalenediimide/multi-wall carbon nanotube and enhanced interfacial properties of high-modulus carbon fiber composites, Compos. Sci. Technol. 184 (2019) 107855.
[36] R. Hao, X. Jiao, X. Zhang, Y. Tian, Fe_3O_4/graphene modified waterborne polyimide sizing agent for high modulus carbon fiber, Appl. Surf. Sci. 485 (2019) 304–313.
[37] J. Zhou, K. Zhong, C. Zhao, H. Meng, L. Qi, Effect of carbon nanotubes grown temperature on the fracture behavior of carbon fiber reinforced magnesium matrix composites: Interlaminar shear strength and tensile strength, Ceram. Int. 47 (2021) 6597–6607.
[38] G. Lee, M. Sung, J.H. Youk, J. Lee, W.-R. Yu, Improved tensile strength of carbon nanotube-grafted carbon fiber reinforced composites, Compos. Struct. 220 (2019) 580–591.

[39] H. Chathuranga, K. Chandula Wasalathilake, I. Marriam, J. MacLeod, Z. Zhang, R. Bai, Z. Lei, Y. Li, Y. Liu, H. Yang, C. Yan, Preparation of Bioinspired Graphene Oxide/PMMA Nanocomposite with Improved Mechanical Properties, Compos. Sci. Technol. 216 (2021) 109046.
[40] Y. Zhang, K. Ruan, J. Gu, Flexible Sandwich-Structured Electromagnetic Interference Shielding Nanocomposite Films with Excellent Thermal Conductivities, Small 17 (2021) 202101951.
[41] Y. Yu, Z. Chao, Q. Gong, C. Li, H. Fu, F. Lei, D. Hu, Tailoring hierarchical carbon nanotube cellular structure for electromagnetic interference shielding in extreme conditions, Mater. Des. 206 (2021) 109783.
[42] N. Chikyu, T. Nakano, G. Kletetschka, Y. Inoue, Excellent electromagnetic interference shielding characteristics of a unidirectionally oriented thin multiwalled carbon nanotube/polyethylene film, Mater. Des. 195 (2020) 108918.
[43] V.T. Nguyen, B.K. Min, Y. Yi, S.J. Kim, C.G. Choi, MXene($Ti_3C_2T_x$)/graphene/PDMS composites for multifunctional broadband electromagnetic interference shielding skins, Chem. Eng. J. 393 (2020) 124608.